ARTICLE OPEN ACCESS

Structural and Clinical Correlates of a Periventricular Gradient of Neuroinflammation in Multiple Sclerosis

Emilie Poirion, PhD, Matteo Tonietto, PhD, François-Xavier Lejeune, PhD, Vito A.G. Ricigliano, MD, Marine Boudot de la Motte, MD, Charline Benoit, MD, Géraldine Bera, MD, Bertrand Kuhnast, PhD, Michel Bottlaender, MD, PhD, Benedetta Bodini, MD, PhD, and Bruno Stankoff, MD, PhD

Correspondence
Dr. Stankoff
bruno.stankoff@aphp.fr

Neurology® 2021;96:e1865-e1875. doi:10.1212/WNL.0000000000011700

Abstract

Objectives

To explore in vivo innate immune cell activation as a function of the distance from ventricular CSF in patients with multiple sclerosis (MS) using [^{18}F]-DPA714 PET and to investigate its relationship with periventricular microstructural damage, evaluated by magnetization transfer ratio (MTR), and with trajectories of disability worsening.

Methods

Thirty-seven patients with MS and 19 healthy controls underwent MRI and [^{18}F]-DPA714 TSPO dynamic PET, from which individual maps of voxels characterized by innate immune cell activation (DPA+) were generated. White matter (WM) was divided in 3-mm-thick concentric rings radiating from the ventricular surface toward the cortex, and the percentage of DPA+ voxels and mean MTR were extracted from each ring. Two-year trajectories of disability worsening were collected to identify patients with and without recent disability worsening.

Results

The percentage of DPA+ voxels was higher in patients compared to controls in the periventricular WM (p = 6.10e-6) and declined with increasing distance from ventricular surface, with a steeper gradient in patients compared to controls (p = 0.001). This gradient was found in both periventricular lesions and normal-appearing WM. In the total WM, it correlated with a gradient of microstructural tissue damage measured by MTR (r_s = −0.65, p = 1.0e-3). Compared to clinically stable patients, patients with disability worsening were characterized by a higher percentage of DPA+ voxels in the periventricular normal-appearing WM (p = 0.025).

Conclusions

Our results demonstrate that in MS the innate immune cell activation predominates in periventricular regions and is associated with microstructural damage and disability worsening. This could result from the diffusion of proinflammatory CSF-derived factors into surrounding tissues.

RELATED ARTICLE

Editorial
Is Cerebrospinal Fluid Responsible for Innate Immune Cell Activation and Neurotoxicity in Multiple Sclerosis?
Page 649

From the Sorbonne University (E.P., M.T., F.-X.L., V.A.G.R., M.B.d.l.M., C.B., G.B., B.B., B.S.), Paris Brain Institute; Imaging Department (E.P.), Foundation A. de Rothschild Hospital, Paris; Paris-Saclay University (M.T., B.K., M.B.), CEA, Orsay; and Assistance Publique des Hôpitaux de Paris (B.B., B.S.), France.

Go to Neurology.org/N for full disclosures. Funding information and disclosures deemed relevant by the authors, if any, are provided at the end of the article.

The Article Processing Charge was funded by Paris Brain Institute, ICM.

Glossary

DPA+ = voxels characterized by a significant activation of innate immune cells; **DVR** = distribution volume ratio; **EDSS** = Expanded Disability Status Scale; **HC** = healthy controls; **MNI** = Montreal Neurological Institute; **MS** = multiple sclerosis; **MT** = magnetization transfer; **MTR** = MT ratio; **PMS** = progressive MS; **pu** = percentage units; **RRMS** = relapsing-remitting MS; **TE** = echo time; **TR** = repetition time; **TSPO** = translocator protein.

Multiple sclerosis (MS) is a complex inflammatory disease responsible for an irreversible CNS injury resulting from a combination of focal lesions and more diffuse structural damage, both contributing to disability worsening.[1]

Recent pathologic investigations have revealed a possible relationship between CSF proximity and microstructural damage in the cortex,[2] potentially related to CSF-derived proinflammatory cytokines.[3] Advanced imaging tools have confirmed that regions facing the CSF are particularly susceptible to tissue damage by showing a correlation between periventricular lesion load and cortical thinning,[4] as well as the presence of a periventricular gradient of microstructural damage.[5–9] Tissue damage in the periventricular white matter has been linked to that of the cortex, suggesting a shared mechanism of injury.[4,5,8,10]

The biological mechanism underlying the relationship between CSF proximity and tissue injury has not been elucidated in vivo yet, but postmortem evidence has suggested an involvement of activated microglial cells.[2] Microglia activation can be visualized with the use of PET with radiotracers targeting the 18-kDa translocator protein (TSPO), the expression of which is upregulated in innate immune cells in inflammatory disorders like MS.[11–17] In this study, we used a high-resolution research tomograph with a fluorinated second-generation TSPO tracer, [^{18}F]-DPA714,[18,19] to explore whether periventricular white matter in MS is characterized by a gradient of innate immune cell activation and to investigate the relationship between this gradient and microstructural damage and disability.

Methods

Standard Protocol Approvals, Registrations, and Patient Consents

All participants signed written informed consent to participate in a clinical and imaging protocol approved by the local ethics committee, according to the Declaration of Helsinki.

Participants

We enrolled 41 patients with MS (13 with relapsing-remitting MS [RRMS], 28 with progressive MS [PMS]) according to the revised McDonald criteria[20] and 20 age- and sex-matched healthy controls (HC).

Genomic DNA from blood samples was used to genotype the rs6971 polymorphism of the TSPO gene,[21] revealing 31 high-affinity binders (22 patients, 9 HC), 25 mixed-affinity binders (15 patients, 10 HC), and 5 low-affinity binders (4 patients, 1 HC). The last group was excluded from further analysis, leaving a total of 37 patients with MS and 19 HC (table 1).

Clinical Assessment

At study entry, all patients underwent a neurologic examination and were scored with the Expanded Disability Status Scale[22] (EDSS). For each patient, the EDSS score 2 years before study entry was collected retrospectively through the careful review of primary medical files and checked for consistency with our local database entered in the European Database for Multiple Sclerosis records. Disability worsening over 2 years was evaluated as changes in EDSS between the inclusion visit and 2 years before study entry and converted into EDSS step change.[23] EDSS step change was used to classify patients as clinically worsening (EDSS step change ≥0.5) or clinically stable over the 2 years preceding study entry. Patients were classified as untreated ("off," if they had no disease-modifying treatment during this period) or treated ("on," if they received a disease-modifying treatment) (table 1 and table e-1, data available from Dryad, doi.org/10.5061/dryad.z612jm69r).

Image Acquisition

Within a maximum of 1 month from study entry, all participants underwent an MRI protocol on a Siemens 3T PRISMA scanner (Siemens, Munich, Germany) equipped with a 32-channel head coil and a 90-minute dynamic [^{18}F]-DPA714 PET examination on a high-resolution research tomograph (CPS Innovations, Knoxville, TN).

The MRI protocol included the following sequences: (1) 3-dimensional T1-weighted magnetization-prepared rapid gradient-echo (repetition time [TR]/echo time [TE]/inversion time 2,300/2.98/900 milliseconds, resolution 1.0 × 1.0 × 1.1 mm^3), (2) T2-weighted imaging (TR/TE 4,500/14 milliseconds, resolution 0.9 × 0.9 × 3.0 mm^3), (3) fluid-attenuated inversion recovery (TR/TE/inversion time 8,880/129/2,500 milliseconds, resolution 0.9 × 0.9 × 3.0 mm^3), and (4) gradient-echo with (MTon) and without (MToff) magnetization transfer (TR/TE 35/5 milliseconds, resolution 1.0 × 1.0 × 2.0 mm^3).

The PET protocol consisted of an IV bolus injection of 198.4 ± 22.9 MBq of [^{18}F]-DPA714 at the beginning of a 90-minute dynamic acquisition, as previously detailed.[24,25] After reconstruction, the resulting dynamic PET images consisted of 27 time interval (time frames) images: six 1-minute frames for

Table 1 Demographic and Clinical Characteristics of Patients With MS and Healthy Controls

Demographic, Clinical, and Radiologic Characteristics	Healthy Controls	Patients With MS (Total)	Relapsing-Remitting MS	Progressive MS
No.	19	37	11	26
Age, y	46.6 ± 14.3	47.7 ± 11.4	42.6 ± 13.3	49.9 ± 10.0
Female/male, n	13/6	21/16	8/3	13/13
Genotype (mixed-/high-affinity binders), n	10/9	15/22	4/7	11/15
Disease duration, y	—	9.3 ± 5.4[a]	6.7 ± 4.4	10.4 ± 5.5
Baseline EDSS score	—	5 (2–7.5)[b]	3.5 (2–6)	6 (3–7.5)
EDSS step change	—	1 (0–4.5)	1 (0–2.5)	1 (0–4.5)
Individual trajectory (clinically stable/clinically worsening), n	—	13/24	4/7	9/17
Disease-modifying treatment (off/on), n	—	20/17[c]	1/10	19/7

Abbreviation: EDSS = Expanded Disability Status Scale; HC = healthy controls; MS = multiple sclerosis.
Values are mean ± SD or median (range).
[a] $p < 0.05$ by Wilcoxon-Mann-Whitney test.
[b] $p < 0.001$ by ordered logistic regression model.
[c] $p < 0.001$ Fisher exact tests between MS subgroups.

the initial 6 minutes (6 × 1), followed by 7 × 2-minute frames and 14 × 5-minute frames, with a spatial resolution of ≈2.5-mm full width at half-maximum.

Image Analysis

Anatomic Image Processing and Generation of Periventricular Concentric Rings

In patients, T2-hyperintense lesions were manually contoured by an expert investigator (G.B.) on T2-weighted scans with reference to fluid-attenuated inversion recovery sequences using a semiautomated edge-finding tool (JIM version 6.0, Xinapse systems, Essex, UK). The corresponding lesion masks were generated and aligned to the individual T1-weighted scans with FLIRT (FMRIB [Oxford Centre for Functional MRI of the Brain, UK] Linear Image Registration Tool, FMRIB Software Library, version 5.0.9).[26] After a lesion-filling procedure in patients only,[27] T1-weighted scans were segmented using a multiatlas segmentation approach[28] and analyzed with FreeSurfer (version 6.0) to calculate the cortical thickness.

The following regions of interest were then defined on T1-weighted scans of all participants: (1) white matter; (2) cortex; and (3) ventricular CSF, including lateral and third ventricles (figure 1, A–C). In patients with MS, the following regions of interest were also defined: T2 lesions and normal-appearing white matter, defined as the white matter outside visible lesions on T2-weighted scans. Manual corrections were performed when necessary to ensure anatomic accuracy. Distance maps from ventricular CSF toward the cortex in the white matter (either total white matter or white matter divided in normal-appearing white matter and T2 lesions) were then calculated as the 3-dimensional euclidean distance to the nearest nonzero voxel (figure 1, D–F).

T1-weighted scans were then normalized to the Montreal Neurological Institute (MNI) 152 standard space with a nonlinear transformation from Advanced Normalization Tools, version 2.2).[29]

Subsequently, all regions of interest and distance maps were aligned to standard space. According to the PET resolution, distance maps were then divided in 3-mm-thick concentric rings, radiating from the ventricular surface toward the cortex (figure 1, D–F). To minimize partial volume effect, the first 3 mm close to ventricles and the last 3 mm close to the white matter/cortex interface were removed from the white matter ring map.

PET Image Processing and Calculation of Innate Immune Cell Activation in Periventricular Concentric Rings

Voxel-wise [^{18}F]-DPA714 distribution volume ratio (DVR) parametric maps (figure 2A) were calculated with the Logan graphical method based on reference region, extracted with a supervised clustering algorithm.[24,30] DVR maps were then aligned using FLIRT[26] to the corresponding T1-weighted images and normalized to the standard space using the previously calculated nonlinear transformations[29] of the T1-weighted in native space onto the MNI152 standard space.

Voxels characterized by innate immune cell activation (hereinafter referred to as DPA+) were identified as those voxels with DVR values that exceeded >20% of the mean DVR

Figure 1 Processing Steps to Generate 3-mm-Thick Ring From CSF to Adjacent White Matter

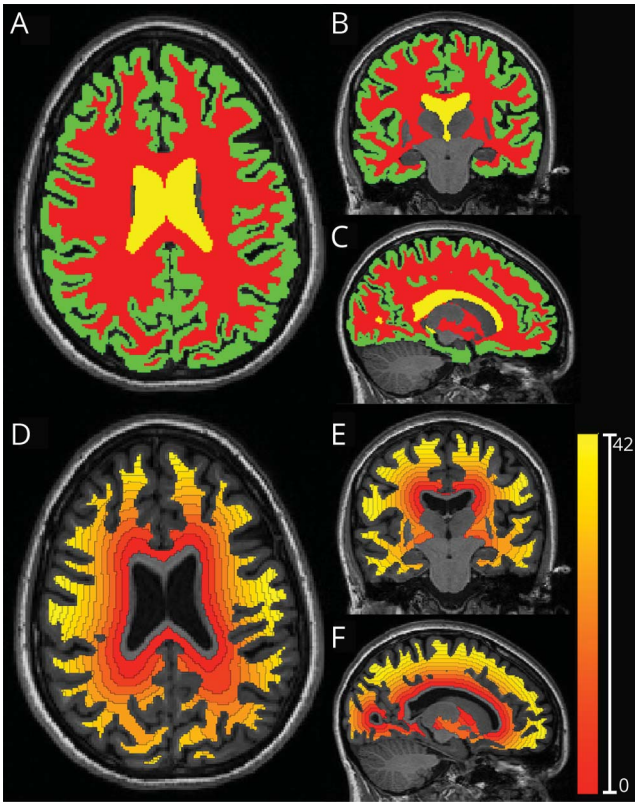

(A–C) Axial, coronal, and sagittal views of a T1-weighted images segmented with a multiatlas segmentation approach generating masks for the white matter, cortex, and ventricles (red, green, and yellow, respectively). (D–F) Axial, coronal, and sagittal views of the corresponding distance map from the ventricular surfaces toward the cortex, calculated in the white matter mask and divided into 3-mm-thick rings.

Figure 2 Illustrative Example of [^{18}F]-DPA714 DVR Maps and the Corresponding Individual Map of DPA+ Voxels

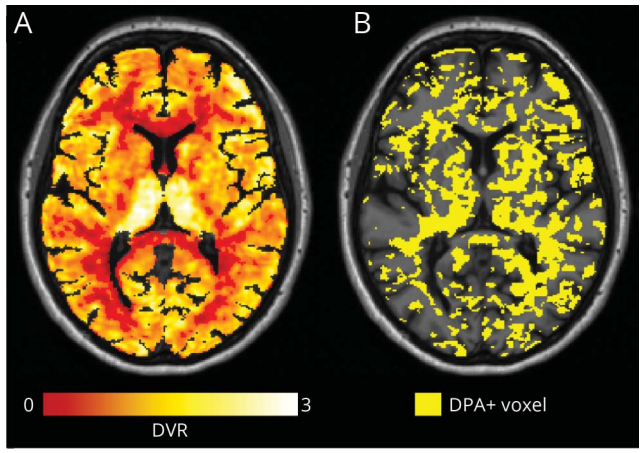

(A) [^{18}F]-DPA714 distribution volume ratio (DVR) map of a representative patient with multiple sclerosis (MS) (45-year-old female patient with secondary progressive MS, disease duration 22 years, Expanded Disability Status Scale [EDSS] score at baseline 6, EDSS step change in the 2 years preceding baseline 1.5). Map was obtained using Logan graphical analysis with reference region extracted with a supervised clustering approach. (B) Corresponding individual map of voxels characterized by a significant activation of innate immune cells (DPA+) (yellow) obtained by thresholding the DVR map of panel A (see text for details about the thresholding technique used).

value of the HC in the same MNI position. The 20% relative threshold had been calculated by means of a voxel-wise nonparametric permutation-based *t* test between the DVR maps of patients and HC, as previously described.[25] This step resulted in the generation of individual maps of innate immune cells activation, consisting of binary masks of DPA+ voxels (figure 2B).

Given the impact of the TSPO affinity on the DVR estimates, voxel classification was conducted separately for high- and mixed-affinity binders.

For each participant, the percentage of voxels classified as DPA+ was extracted from each ring of the white matter and of T2 lesions and normal-appearing white matter separately in patients only.

MT Ratio in Periventricular Concentric Rings

For each participant, both MToff and MTon sequences were rigidly aligned[26] to the corresponding T1-weighted scan in native space. Maps of MT ratio (MTR) were calculated as MTR = (MToff − MTon)/MToff, measured in percentage units (pu), and normalized to the standard space with the previously calculated transformations. In all participants, mean MTR values within each ring of the white matter were extracted.

Due to the presence of artifacts, the MTR images of 9 participants (4 patients, 5 HC) were excluded from further MTR-based analysis, leaving a total of 33 patients (women n = 19, age 48.1 ± 11.6 years) and 14 HC (women n = 9, age 41.0 ± 12.4 years).

Statistical Analysis

Statistical analyses were performed with R (R Foundation for Statistical Computing, version 3.5.0, Vienna, Austria). Demographic and clinical data are presented as mean ± SD, while EDSS score and EDSS step change are presented as median (range). For inferential statistics, results are reported as mean ± SD, except when specified otherwise. For all tests, the level of statistical significance was set at $p < 0.05$, and pairwise comparisons of estimated marginal means were performed with Bonferroni correction when necessary.

Wilcoxon-Mann-Whitney tests were used to assess differences in age between HC and patients with MS and in disease duration between patients with RRMS and those with PMS. Fisher exact tests were used to determine whether there were significant differences in the proportion of sex and TSPO genotype between HC and patients with MS and treatment and disability worsening category among patients with RRMS

Figure 3 Periventricular Gradient of Innate Immune Cell Activation in the WM of Patients With MS

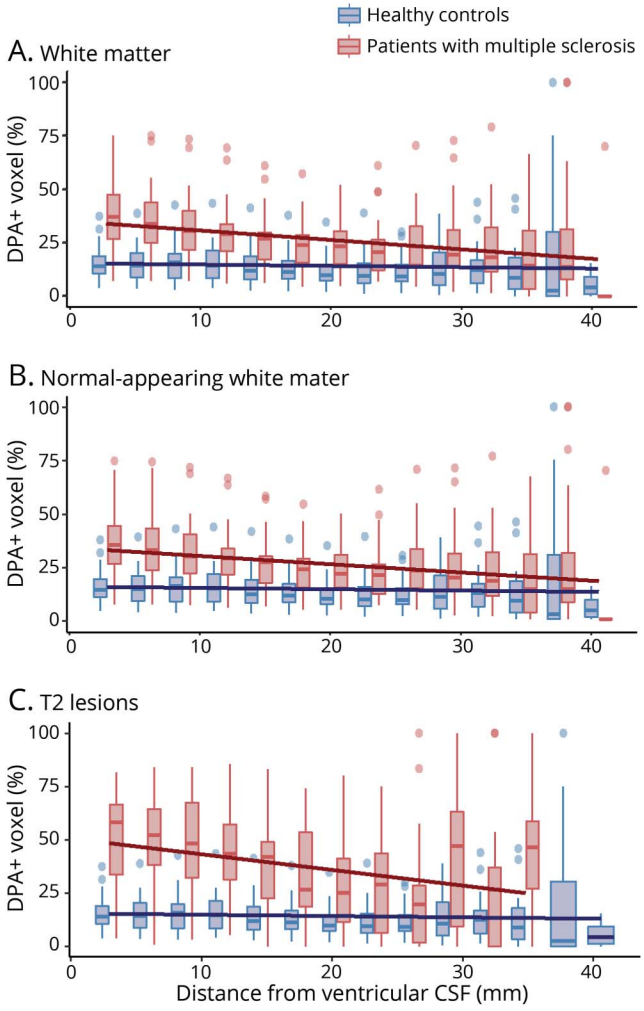

Boxplots represent the percentage of voxels characterized by a significant activation of innate immune cells (DPA+) in (A) the total white matter (WM), (B) the normal-appearing WM, and (C) T2 lesions in patients with multiple sclerosis (MS) (red) and in the WM of healthy controls (blue), calculated in 3-mm-thick concentric rings radiating from the ventricular CSF toward the cortex. Solid lines represent the mixed-effect model fits obtained at the population level for both groups.

and PMS. Ordered logistic regression models were used to test differences in EDSS and EDSS step changes between RRMS and PMS.

Relationship Between Innate Immune Cell Activation and Distance From Ventricular CSF

To evaluate the relationship between the percentage of DPA+ voxels, reflecting innate immune cell activation, and the distance from the ventricular CSF, we used 3 separate linear mixed-effects models (package lme4) for the whole white matter, normal-appearing white matter, and T2 lesions. Each model included the percentage of DPA+ voxels in each ring as the dependent variable and the following independent variables: (1) ring distance from CSF, (2) group (HC or patients with MS), and (3) interaction between ring distance from CSF and group. To further investigate the contribution of T2 lesions to the spatial distribution of DPA+ voxels in the normal-appearing white matter, we used an additional linear mixed-effects model in patients only in which the percentage of DPA+ voxels in the normal-appearing white matter was included as a dependent variable and the ring distance from CSF and percentage of lesional voxels in each ring were included as independent variables. In all models, participants and ring distance from CSF were considered random effects to account for participant variability. Because the percentages of DPA+ voxels were calculated in rings with different volumes, we assigned a weight to each data point corresponding to the number of voxels used to calculate each percentage, reflecting the degree of precision of each data point. As a result, percentages calculated on few voxels (i.e., rings near cortex due to presence of cortical gyri) had a low impact on the model fit.

In these models, the relationship between the percentage of DPA+ voxels and the ring distance from the ventricular CSF was described by the intercept and slope parameters of a linear model: an intercept represents the estimated percentage of DPA+ voxels, reflecting the extent of activated innate immune cells, at the closest proximity to the CSF; and a slope reflects the rate of change in the percentage of DPA+ voxels with distance from the ventricles. Both parameters were obtained as linear combinations of the model coefficients, which were simultaneously estimated at both the population level (e.g., in HC and patients with MS) and the single-participant level.

For each model, differences of intercept and slope between HC and patients with MS were tested with *t* tests on the estimated population parameters.

To compare the relationship between the percentage of DPA+ voxels and the distance from the ventricular CSF between MS subgroups (RRMS and PMS) and HC in white matter, normal-appearing white matter, and T2 lesions, linear regression models were used, including the intercept and slope parameters estimated at the single-participant level as dependent variables and group with the covariates age, sex, and presence of disease-modifying treatment as independent variables.

Relationship Between Innate Immune Cell Activation and Microstructural Damage

An identical statistical procedure to that described above for the innate immune cell activation was then repeated to describe the relationship between MTR values, reflecting microstructural damage, and the distance from ventricular CSF in the white matter. In this case, each model returned the following parameters: an intercept, reflecting the estimated MTR value at the closest proximity to the CSF, and a slope, representing the rate of change in MTR values with distance from the ventricles. These parameters were simultaneously estimated at the population level and at the single-participant level.

To investigate whether the innate immune cell activation was associated with microstructural damage at the closest

Table 2 [^{18}F]-DPA714 PET- and MTR-Derived Measurements at the Population Level

	DPA+ Voxel						MTR	
	White Matter		Normal-Appearing White Matter		T2 Lesions		White Matter	
Participants Group	Intercept, %	Slope, %·mm^{-1}	Intercept, %	Slope, %·mm^{-1}	Intercept, %	Slope, %·mm^{-1}	Intercept, pu	Slope, pu·mm^{-1}
HC	17.42 ± 9.66	−0.22 ± 0.22					47.05 ± 1.05	−0.049 ± 0.017
MS	39.01 ± 17.15	−0.76 ± 0.62	37.01 ± 16.52	−0.67 ± 0.54	53.28 ± 21.88	−0.78 ± 0.72	44.63 ± 2.16	0.044 ± 0.068
RRMS	33.32 ± 16.12	−0.70 ± 0.73	31.15 ± 15.10	−0.60 ± 0.63	50.51 ± 22.38	−0.72 ± 0.86	45.05 ± 2.06	0.044 ± 0.050
PMS	41.42 ± 17.31	−0.79 ± 0.58	39.48 ± 16.74	−0.70 ± 0.51	54.44 ± 22.01	−0.81 ± 0.67	44.45 ± 2.22	0.044 ± 0.075
Stable	30.68 ± 14.33	−0.61 ± 0.54	28.58 ± 13.30	−0.51 ± 0.46	46.56 ± 24.42	−0.67 ± 0.74	44.97 ± 1.63	0.029 ± 0.039
Worsening	43.52 ± 17.12	−0.85 ± 0.65	41.57 ± 16.52	−0.75 ± 0.58	56.91 ± 19.97	−0.84 ± 0.72	44.44 ± 2.43	0.053 ± 0.080

Abbreviations: DPA+ = voxels characterized by a significant activation of innate immune cells; HC = healthy controls; MS = multiple sclerosis; MTR = magnetization transfer ratio; PMS = progressive MS; pu = percentage units; RRMS = relapsing-remitting MS.

proximity to the CSF in white matter, we used partial Spearman correlations between the intercepts of single-patient percentage of DPA+ voxels and mean MTR, adjusted for age, sex, and presence of disease-modifying treatment.

To assess whether the rate of change in innate immune cell activation with distance from the ventricles was associated with the rate of change in microstructural damage in white matter, we used partial Spearman correlations between the slopes of single-patient percentage of DPA+ voxels and mean MTR, adjusted for age, sex, and presence of disease-modifying treatment.

Spatial Distribution of Innate Immune Cell Activation: Relationship With Cortical Thickness and Clinical Scores

We investigated the relationship between DPA+ voxel intercept and slope in periventricular areas (white matter, normal-appearing white matter, and T2 lesions) and cortical thickness using partial Spearman correlations and their difference between clinically worsening and clinically stable patients using linear regression models. All analyses were adjusted for age, sex, and presence of disease-modifying treatment.

The differences between clinically worsening and clinically stable patients in the percentage of DPA+ voxels intercepts and slopes in periventricular areas (white matter, normal-appearing white matter, and T2 lesions) were tested with linear regression models adjusted for age, sex, and presence of disease-modifying treatment.

Data Availability

The data that support the findings of this study are available from the corresponding author on reasonable request.

Results

Demographics

Demographic and clinical characteristics of the recruited participants are reported in table 1. No significant differences were found between HC and patients with MS in age (p = 0.96), sex (p = 0.56), and TSPO genotype (p = 0.41).

Patients With MS Show a Periventricular Gradient of Innate Immune Cell Activation

Patients with MS had a higher percentage of DPA+ voxels compared to HC in the white matter at the closest proximity to the ventricles (intercept for patients 39.0 ± 17.2%, intercept for HC 17.4 ± 9.7%, t = 5.01, p = 6.10e-6; figure 3A and table 2). The percentage of DPA+ voxels decreased −0.76 ± 0.62% (t = −7.00, p = 3.39e-8) for each 1 mm of distance from the CSF in patients with MS, while it remained stable in HC (slope for HC −0.22 ± 0.22% · mm^{-1}, t = −1.73, p = 0.090), resulting in a significant difference between the gradient in the 2 groups of −0.54 ± 0.16%·mm^{-1} (mean ± standard error, t = −3.46, p = 0.001).

A similar regional distribution of innate immune cell activation was found when normal-appearing white matter and T2 lesions were analyzed separately (figure 3, B and C, respectively). Compared to the white matter of HC, patients with MS showed a higher percentage of DPA+ voxels at the closest proximity to the ventricles and a steeper slope in both normal-appearing white matter (intercept 37.0 ± 16.5%, t = 4.70, p = 1.83e-5; slope −0.67 ± 0.54%·mm^{-1}, t = −3.19, p = 2.37e-3) and T2 lesions (intercept 53.3 ± 21.9%, t = 6.50, p = 5.09e-8; slope −0.78 ± 0.72%·mm^{-1}, t = −2.49, p = 0.018) (table 2). Moreover, in the normal-appearing white matter of patients with MS, the percentage of DPA+ voxels was found to be associated not only with the distance from ventricles but also with the percentage of lesional voxels in each

Figure 4 Relationship Between Innate Immune Cell Activation and MTR in the Periventricular WM

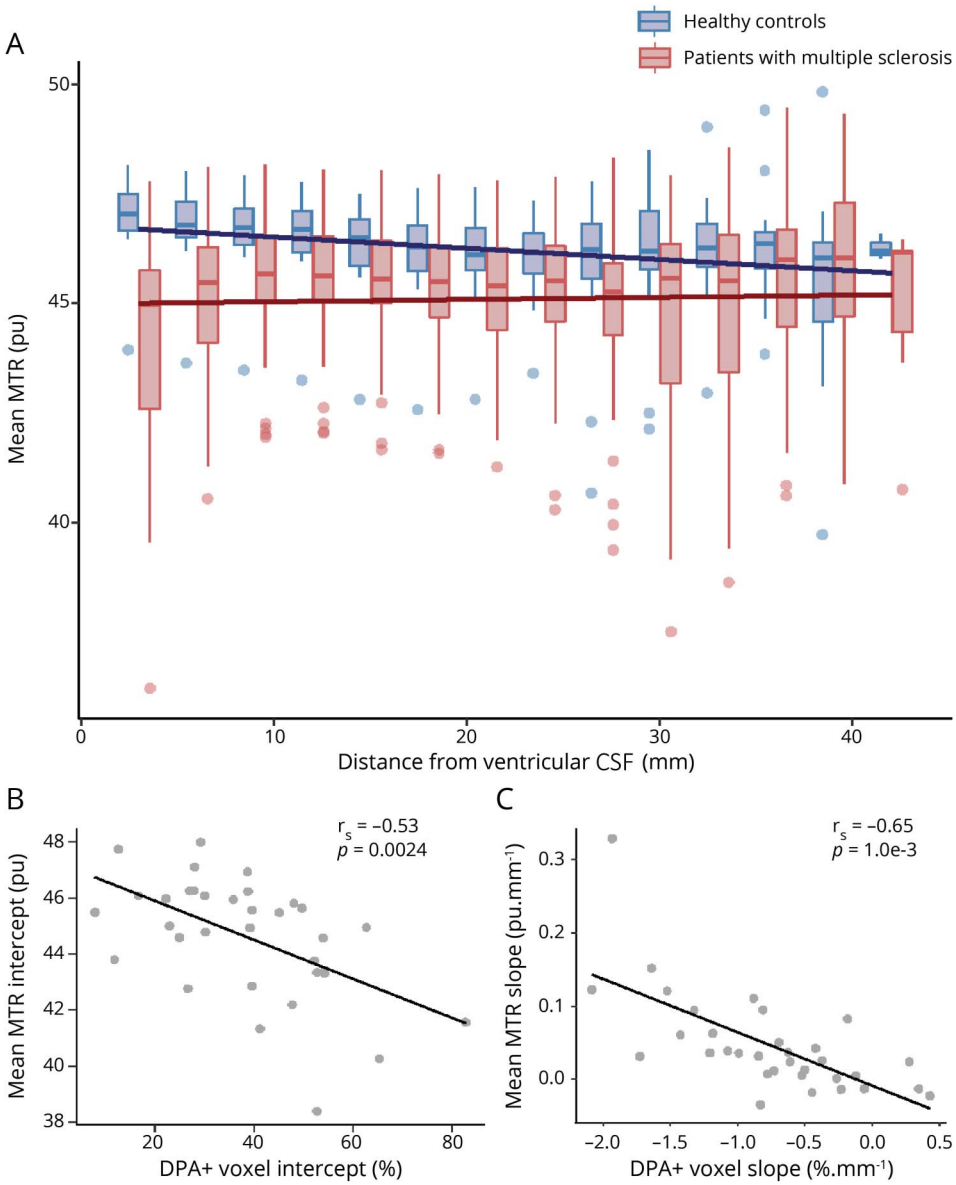

(A) Boxplots represent the mean magnetization transfer ratio (MTR) in the white matter (WM) of healthy controls (blue) and patients with multiple sclerosis (MS) (red) calculated in 3-mm-thick concentric rings radiating from the ventricular CSF toward the cortex. Solid lines represent the mixed-effect model fits obtained at the population level for both healthy controls and patients with MS. In WM, both (B) the intercepts and (C) the slopes of the percentage of voxels characterized by a significant activation of innate immune cells (DPA+) and mean MTR values were inversely correlated with each other.

periventricular ring (t = −5.59, p = 1.64e-6; t = 6.63, p = 1.00e-10; respectively).

When we performed the patient subgroup analysis, while the patients with PMS showed a higher level of innate immune cell activation in the periventricular white matter, normal-appearing white matter, and T2 lesions and steeper slopes compared to patients with RRMS, these differences were not statistically significant (table 2 and table e-2, data available from Dryad, doi.org/10.5061/dryad.z612jm69r).

Association Between Innate Immune Cell Activation and Microstructural Damage in Periventricular White Matter

In white matter, patients with MS had a lower mean MTR compared to HC at the closest proximity to the ventricles (intercept for patients 44.6 ± 2.2 pu, intercept for HC 47.1 ± 1.1 pu, t = −3.88, p = 3.37e-4; figure 4A and table 2). The mean MTR increased 0.044 ± 0.068 pu (t = 3.12, p = 3.89e-3) for each 1 mm of distance from the CSF in patients with MS, while it decreased 0.049 ± 0.017 pu (t = −2.70, p = 0.01) in HC, resulting in a significant difference between the 2 groups of 0.093 ± 0.022 pu·mm^{-1} (mean ± standard error, t = 4.27, p = 1.09e-04).

In patients with MS, a higher percentage of DPA+ voxels was significantly associated with a lower mean MTR at the closest proximity to ventricular CSF (r_s = −0.53, p = 0.0024) (figure 4B). Moreover, the decreasing rate of the percentage of DPA+ voxels with distance from the ventricles was associated with a corresponding increasing rate of mean MTR (r_s = −0.65, p = 1.0e-3) (figure 4C).

Periventricular Activation of Innate Immune Cells Is Associated With Cortical Thickness and Is Higher in Clinically Worsening Patients

The association between a higher percentage of DPA+ voxels at the closest proximity to ventricular CSF and a reduced cortical thickness was not significant in the total white matter (r_S = −0.33, p = 0.058). However, this association was significant in the normal-appearing white matter (r_s = −0.34, p = 0.0497) but not in T2 lesions (r_s = −0.25, p = 0.15). The decreasing rate of the percentage of DPA+ voxels with distance from the ventricles was not associated with the cortical thickness (white matter: r_s = 0.20, p = 0.27; normal-appearing white matter: r_s = 0.23, p = 0.19; T2 lesions: r_s = 0.17, p = 0.33).

Compared to patients who remained stable over the 2 years preceding study entry, clinically worsening patients had a significantly higher percentage of DPA+ voxels at the closest proximity to ventricular CSF in the whole white matter (intercept for clinically worsening patients 43.5 ± 17.1%, intercept for clinically stable patients 30.7 ± 14.3%, t = 2.20, p = 0.035; figure 5A). The difference in the slopes between clinically worsening and clinically stable patients was not significant (slope for clinically worsening patients −0.85 ± 0.65%·mm^{-1}, slope for clinically stable patients −0.61 ± 0.54%·mm^{-1}, t = −1.29, p = 0.21).

When normal-appearing white matter and T2 lesions were analyzed separately, clinically worsening patients showed a higher percentage of DPA+ voxels at the closest proximity to the ventricles only in the normal-appearing white matter (intercept for clinically worsening patients 41.6 ± 16.5%, intercept for clinically stable patients 28.6 ± 13.3%, t = 2.35, p = 0.025; figure 5B) but not in T2 lesions (intercept for clinically worsening patients 56.9 ± 20.0%, intercept for clinically stable patients 46.6 ± 24.4%, t = 1.21, p = 0.24; figure 5C). The difference in the rate of decrease in the percentage of DPA+ voxels with distance from the ventricular CSF was not significant between clinically worsening and clinically stable patients in the normal-appearing white matter (slope for clinically worsening patients −0.75 ± 0.58%·mm^{-1}, slope for clinically stable patients −0.51 ± 0.46%·mm^{-1}, t = −1.50, p = 0.14), nor in T2 lesions (slope for clinically worsening patients −0.84 ± 0.72%·mm^{-1}, slope for clinically stable patients −0.67 ± 0.74%·mm^{-1}, t = −0.60, p = 0.55).

Figure 5 Periventricular Innate Immune Cells Activation Associates With Clinical Trajectories of Disability Worsening

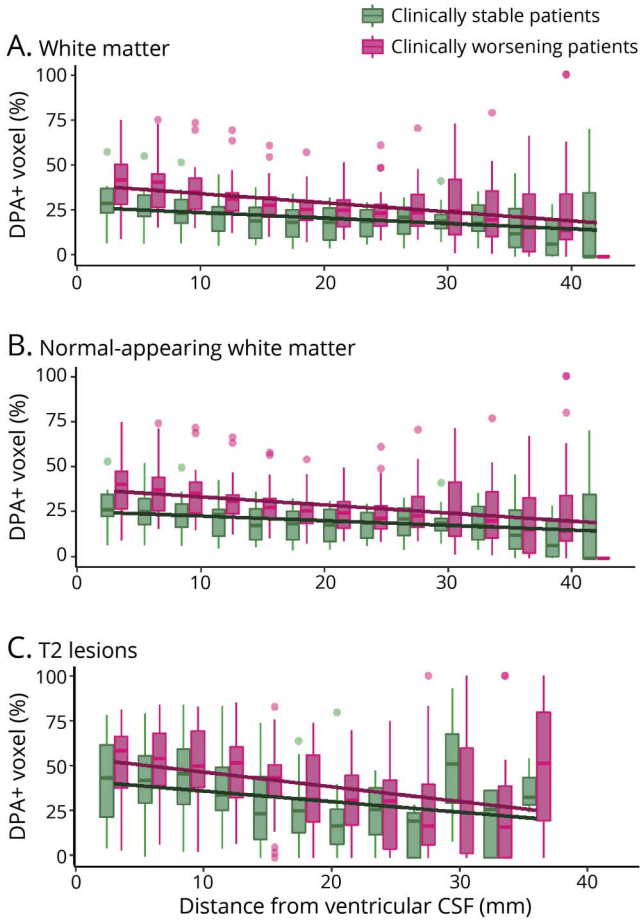

Boxplots represent the percentage of voxels characterized by a significant activation of innate immune cells (DPA+) in (A) the total white matter, (B) the normal-appearing white matter, and (C) T2 lesions of clinically stable patients (green) and clinically worsening patients (pink) calculated in 3-mm-thick concentric rings radiating from the ventricular CSF toward the cortex. Solid lines represent the mixed-effect model fits obtained at the population level for both groups.

Discussion

In this study, we generated individual maps of TSPO binding based on [^{18}F]-DPA714 PET to explore the regionalization of activated innate immune cells as a function of the distance from ventricular surface in a group of patients with MS compared with HC. We demonstrated that in patients with MS the innate immune cell activation was higher at the closest proximity to the ventricular CSF and declined with increasing distance from the ventricles, particularly in clinically worsening compared to clinically stable patients. Moreover, we found that the decreasing rate of active innate immune cells with distance from the ventricles was associated with a corresponding increase in the rate of microstructural damage, as measured by MTR.

Several biological mechanisms may underlie the particular brain regionalization of innate immune cell activation and corresponding microstructural damage that we found in our study in patients with MS. Periventricular tissues are known to be a preferential localization of MS plaques that originate from an acute adaptive immunity response around postcapillary veins.[31] Subsequent upregulation and downregulation of lymphocytes T and B surface molecules were identified as a potential mechanism driving the persistence and compartmentalization of the inflammatory response in some established lesions.[32,33] This compartmentalized inflammation may

result in the secretion of proinflammatory mediators that could diffuse in surrounding periventricular areas and induce a persistent activation of innate immune cells. One interesting candidate molecular signal could be fibrine, which has been shown to be able to invade the perivenular space and to promote the activation of microglia and the recruitment of peripheral inflammatory macrophages into the CNS.[34,35]

In our study, when looking separately at normal-appearing white matter and T2 lesions in periventricular regions, we found a gradient of innate immune cell activation in both compartments. This higher activation of innate immune cells might therefore also be explained by the diffusion of soluble factors localized in the CSF, which could exert a deleterious role on tissues localized near the inner surface of the brain, both inside and outside demyelinating lesions. CSF-derived soluble factors from patients with MS have already been shown to induce neuronal damage in vitro,[36] with a few candidate molecules identified such as ceramide,[37] semaphorine 4A,[38] and HERV-W Env proteins.[39] An increased level of proinflammatory cytokines in the CSF of postmortem cases of MS (interferon-γ, tumor necrosis factor, interleukin-2, interleukin-22, chemokine [C-X-C motif] ligand 13 and 10, lymphotoxin-α, interleukin-6, interleukin-10) was also shown to correlate with meningeal inflammation and extended gray matter tissue damage in subpial cortical regions.[3] A regionalization of innate immune cell activation in cortical regions facing the inflamed CSF, which was spatially associated with enhanced demyelination and neuronal death in the outer cortical layers, was also described in postmortem samples.[2,3,40–42] Because the CSF is a highly dynamic compartment with large exchanges between the subarachnoid space and the ventricles, our results could suggest that a mechanism similar to the one at play in cortical regions facing the CSF may also underlie the severe microstructural damage affecting periventricular white matter. In addition, the infiltration of inflammatory cells through the more permeable blood-to-CSF barrier has been described as an early and sustained event in the experimental autoimmune encephalitis model of MS.[43,44] Whereas their number is generally mild, the long-lasting presence of inflammatory cells in the CSF compartment of patients with MS could also contribute to the pathologic process, enhancing the parenchymal infiltration of immune cells and/or inducing a diffuse damage in tissues adjacent to the CSF, that is, periventricular areas and subpial cortex. According to these hypotheses, inflammatory/cytotoxic mediators and/or inflammatory cells released in the CSF would induce a gradient of innate immune cells activation in surrounding tissues. It is possible, however, that in the normal-appearing white matter this gradient depends from the proximity to both CSF and white matter lesions; we found an independent contribution of the distance from ventricles and of T2 lesions to the spatial distribution of DPA+ voxels.

Whatever the mechanism underlying the selective periventricular activation of innate immune cells may be, this gradient provides one explanation for the predominant tissue loss described in the same region by MRI[4–6,8,10] because a significant correlation between the periventricular gradient of innate immune cell activation and that of microstructural damage in the white matter was shown.

Although these hypotheses should be further explored by future experimental and pathologic studies, a novel concept of the mechanisms underlying tissue damage in MS could be proposed in which periventricular innate immune cell activation plays a key role in the cascade of events leading to neurodegeneration and ultimately to disease progression. Our results are in line with previously published data highlighting the clinical relevance of the periventricular gradient of microstructural damage specifically characterizing the normal-appearing white matter.[6] We found a significant association between periventricular neuroinflammation, disability trajectories, and cortical damage in the normal-appearing white matter only, suggesting that the contribution of innate immune system to neurodegeneration may not be restricted to a more destructive fate or a lack of repair within MS lesions. How neuroinflammation in the periventricular regions could ultimately result in tissue damage and neurologic disability remains unclear, but the cascade of events may potentially involve oxidative and energetic dysregulation, followed by wallerian or dying-back axonal degeneration.[45]

This study has potential limitations that should be taken into account in the interpretation of results. First, TSPO PET tracers have a suboptimal specificity for innate immune cells because they can also bind to reactive astrocytes and endothelial cells.[46–48] Postmortem evidence has indicated that TSPO+ vascular endothelium accounted for <5% of the TSPO+ cells, with no difference in vascular expression between patients with MS and HC in the white matter.[47] These findings, together with the methodology used to identify DPA+ voxels that classifies each voxel according to the mean binding found in the same voxel of a group of controls, argue for a negligible bias induced by the vascular binding in our study. In contrast, in active lesions and in the rim of chronic active lesions, astrocytes constitute up to 25% of TSPO-expressing cells,[47] and our methodology does not allow discriminating between the innate immune and the astrocytic contribution underlying the increased binding of [^{18}F]-DPA714. Further studies are therefore needed to check whether TSPO expression in astrocytes is indeed linked to a proinflammatory state, contributing with microglial cells to the deleterious neuroinflammatory environment in MS, as already shown in the experimental allergic encephalomyelitis model.[49]

Another limitation is that TSPO tracers do not currently allow the differentiation between proinflammatory and regulatory innate immune cells.[47] However, the correlation found between a higher activation of innate immune cells and a more severe microstructural damage in the periventricular region, together with the neuropathologic evidence that in MS lesions homeostatic microglial cells are downregulated while proinflammatory microglial cells predominate,[33] suggest that the TSPO binding detected in this study might reflect mainly the activation of proinflammatory innate immune cells.

Finally, the cross-sectional design of our imaging study does not allow us to establish whether the periventricular gradient of innate immune activation chronologically follows or precedes (and is therefore potentially responsible for) the gradient of microstructural damage demonstrated with MTR. Moreover, we cannot fully exclude that part of the periventricular gradient of MTR change is directly linked to inflammation because MTR was shown to be sensitive to neuroinflammation.[50] Therefore, only longitudinal prospective studies combining imaging markers of innate immune cell activation and microstructural damage would have the potential to define the exact sequence of pathologic events and to identify the predictive value of the periventricular gradient of innate immune cell activation in the development of brain atrophy and disability progression.

Of note, the moderate quality of some MT acquisition has led to the exclusion of some participants from the MTR analysis, limiting the investigation of the relationship between innate immune cell action and microstructural damage to a subsample of our data, including 33 patients and 14 HC. Because the MT acquisition consists of 2 acquisitions, with and without the MT pulse, particular caution should be taken with the registration between them, as well as movement artifacts that might compromise data.

In conclusion, we were able to identify a pathologic substrate for the periventricular gradient of microstructural damage that characterizes MS, consisting of a gradient of innate immune cell activation, reflected by [^{18}F]-DPA714 binding. In combination with previous postmortem investigations, these results suggest that tissue pathology in MS occurs preferentially at or near the inner surface of the brain and is possibly linked to the proximity to the ventricular CSF and mediated by innate immune cell activation. Further work is needed to clarify the potential role of factors such as CSF mediators and intrathecal inflammation in the pathogenesis of lesional and nonlesional abnormalities in MS.

Acknowledgment

The authors thank the Centre d'Investigation Clinique (CIC) team from the Paris Brain Institute (ICM); Céline Louapre and Jean-Christophe Corvol for protocol organization; Caroline Papeix, Catherine Lubetzki, Elizabeth Maillart, and Rana Assouad for helpful discussion and clinical help; and C Baron, C Manciot, Vincent Lebon (Service Hospitalier Frederic Joliot, Commissariat à l'énergie atomique et aux énergies alternatives (SHFJ, CEA)), and Geraldine Gourbil (CIC) for their invaluable assistance. The authors send special thanks to Mattia Veronese, Federico Turkheimer for technical help and fruitful discussions. They also thank the staff of the CENIR (Research Neuroimaging Unit of the ICM) and the staff of the Unité de Recherche Clinique of Pitié Salpêtrière, in particular Anne Bissery and Laura Morizot.

Study Funding

Study funding by the Agence Nationale de la Recherche, grant MNP2008-007125 to B.S. Additional funding from Fondation pour l'aide à la recherche sur la sclérose en plaques (ARSEP Foundation), European Committee for Treatment and Research in Multiple Sclerosis (ECTRIMS), Journées de Neurologie de Langue Française, and Fondation pour la Recherche Médicale. Assistance Publique des Hôpitaux de Paris sponsored the Study.

Disclosure

Dr. Poirion, Dr. Tonietto, Dr. Lejeune, Dr. Ricigliano, Dr. Boudot de la Motte, Dr. Benoit, Dr. Bera, Dr. Kuhnast, and Dr. Bottlaender report no disclosures. Dr Bodini reports fees for traveling and speaker's honoraria from Novartis, Genzyme, Roche, and Merck Serono, all outside the submitted work. Dr. Stankoff reports grants and personal fees for lectures from Roche, Sanofi-Genzyme, and Merck-Serono, as well as personal fees for lectures from Novartis, Biogen, and Teva, all outside the submitted work. Go to Neurology.org/N for full disclosures.

Publication History

Received by *Neurology* June 8, 2020. Accepted in final form January 4, 2021.

Appendix Authors

Name	Location	Contribution
Emilie Poirion, PhD	Paris Brain Institute, Paris, France	Design and conceptualized study; major role in the acquisition of data; analyzed the data; interpreted the data; performed statistical analysis, drafted the manuscript for intellectual content
Matteo Tonietto, PhD	Paris Brain Institute, Paris, France	Analyzed the data; interpreted the data; reviewed statistical analysis, drafted the manuscript for intellectual content
François-Xavier Lejeune, PhD	Paris Brain Institute, Paris, France	Analyzed the data, reviewed statistical analysis
Vito A.G. Ricigliano, MD	Paris Brain Institute, Paris, France	Analyzed the data
Marine Boudot de la Motte, MD	Paris Brain Institute, Paris, France	Analyzed the data
Charline Benoit, MD	Paris Brain Institute, Paris, France	Analyzed the data
Géraldine Bera, MD	Paris Brain Institute, Paris, France	Major role in the acquisition of data
Bertrand Kuhnast, PhD	CEA, Orsay, France	Major role in the acquisition of data
Michel Bottlaender, MD, PhD	CEA, Orsay, France	Design and conceptualized study; major role in the acquisition of data
Benedetta Bodini, MD, PhD	Paris Brain Institute, Paris, France	Design and conceptualized study; interpreted the data; drafted the manuscript for intellectual content

Appendix *(continued)*

Name	Location	Contribution
Bruno Stankoff, MD, PhD	Paris Brain Institute, Paris, France	Obtained funding for the study; designed and conceptualized study; interpreted the data; drafted the manuscript for intellectual content

References

1. Lassmann H. Pathogenic mechanisms associated with different clinical courses of multiple sclerosis. Front Immunol 2019;9:3116.
2. Magliozzi R, Howell OW, Reeves C, et al. A gradient of neuronal loss and meningeal inflammation in multiple sclerosis. Ann Neurol 2010;68:477–493.
3. Magliozzi R, Howell OW, Nicholas R, et al. Inflammatory intrathecal profiles and cortical damage in multiple sclerosis. Ann Neurol 2018;83:739–755.
4. Jehna M, Pirpamer L, Khalil M, et al. Periventricular lesions correlate with cortical thinning in multiple sclerosis: cortical thinning and periventricular lesions in MS. Ann Neurol 2015;78:530–539.
5. Brown JW, Chowdhury A, Kanber B, et al. Magnetisation transfer ratio abnormalities in primary and secondary progressive multiple sclerosis. Mult Scler J 2020;26:679–687.
6. Brown JWL, Pardini M, Brownlee WJ, et al. An abnormal periventricular magnetization transfer ratio gradient occurs early in multiple sclerosis. Brain 2017;140:387–398.
7. Liu Z, Pardini M, Ö Yaldizli, et al. Magnetization transfer ratio measures in normal-appearing white matter show periventricular gradient abnormalities in multiple sclerosis. Brain 2015;138:1239–1246.
8. Pardini M, Sudre CH, Prados F, et al. Relationship of grey and white matter abnormalities with distance from the surface of the brain in multiple sclerosis. J Neurol Neurosurg Psychiatry 2016;87:1212–1217.
9. Fadda G, Brown RA, Magliozzi R, et al. A surface-in gradient of thalamic damage evolves in pediatric multiple sclerosis. Ann Neurol 2019;85:340–351.
10. Pardini M, Petracca M, Harel A, et al. The relationship between cortical lesions and periventricular NAWM abnormalities suggests a shared mechanism of injury in primary-progressive MS. Neuroimage Clin 2017;16:111–115.
11. Airas L, Nylund M, Rissanen E. Evaluation of microglial activation in multiple sclerosis patients using positron emission tomography. Front Neurol 2018;9:181.
12. Banati R, Newcombe J, Gunn RN, et al. The peripheral benzodiazepine binding site in the brain in multiple sclerosis. quantitative in vivo imaging of microglia as a measure of disease activity. Brain 2000;123:2321–2337.
13. Stankoff B, Poirion E, Tonietto M, Bodini B. Exploring the heterogeneity of MS lesions using positron emission tomography: a reappraisal of their contribution to disability. Brain Pathol Zurich Switz 2018;28:723–734.
14. Datta G, Colasanti A, Kalk N, et al. 11C-PBR28 and 18F-PBR111 detect white matter inflammatory heterogeneity in multiple sclerosis. J Nucl Med 2017;58:1477–1482.
15. Politis M, Giannetti P, Su P, et al. Increased PK11195 PET binding in the cortex of patients with MS correlates with disability. Neurology 2012;79:523–530.
16. Rissanen E, Tuisku J, Rokka J, et al. In vivo detection of diffuse inflammation in secondary progressive multiple sclerosis using PET imaging and the radioligand 11C-PK11195. J Nucl Med 2014;55:939–944.
17. Herranz E, Giannì C, Louapre C, et al. The neuroinflammatory component of gray matter pathology in multiple sclerosis. Ann Neurol 2016;80:776–790.
18. James ML, Fulton RR, Vercoullie J, et al. DPA-714, a new translocator protein-specific ligand: synthesis, radiofluorination, and pharmacologic characterization. J Nucl Med 2008;49:814–822.
19. Rizzo G, Veronese M, Tonietto M, et al. Generalization of endothelial modelling of TSPO PET imaging: considerations on tracer affinities. J Cereb Blood Flow Metab 2019;39:874–885.
20. Polman CH, Reingold SC, Banwell B, et al. Diagnostic criteria for multiple sclerosis: 2010 revisions to the McDonald criteria. Ann Neurol 2011;69:292–302.
21. Owen DRJ, Gunn RN, Rabiner EA, et al. Mixed-affinity binding in humans with 18-kDa translocator protein ligands. J Nucl Med 2011;52:24–32.
22. Kurtzke JF. Rating neurologic impairment in multiple sclerosis: an Expanded Disability Status Scale (EDSS). Neurology 1983;33:1444–1452.
23. Weinshenker BG, Issa M, Baskerville J. Meta-analysis of the placebo-treated groups in clinical trials of progressive MS. Neurology 1996;46:1613–1619.
24. García-Lorenzo D, Lavisse S, Leroy C, et al. Validation of an automatic reference region extraction for the quantification of [18F] DPA-714 in dynamic brain PET studies. J Cereb Blood Flow Metab 2017;38:333–346.
25. Bodini B, Poirion E, Tonietto M, et al. Individual mapping of innate immune cell activation is a candidate marker of patient-specific trajectories of disability worsening in multiple sclerosis. J Nucl Med 2020;61:1043–1049.
26. Jenkinson M, Smith S. A global optimisation method for robust affine registration of brain images. Med Image Anal 2001;5:143–156.
27. Chard DT, Jackson JS, Miller DH, Wheeler-Kingshott CAM. Reducing the impact of white matter lesions on automated measures of brain gray and white matter volumes. J Magn Reson Imaging 2010;32:223–228.
28. Wang H, Suh JW, Das SR, Pluta JB, Craige C, Yushkevich PA. Multi-atlas segmentation with joint label fusion. IEEE Trans Pattern Anal Mach Intell 2013;35:611–623.
29. Avants BB, Epstein CL, Grossman M, Gee JC. Symmetric diffeomorphic image registration with cross-correlation: evaluating automated labeling of elderly and neurodegenerative brain. Med Image Anal 2008;12:26–41.
30. Lavisse S, García-Lorenzo D, Peyronneau M-A, et al. Optimized quantification of translocator protein radioligand 18F-DPA-714 uptake in the brain of genotyped healthy volunteers. J Nucl Med 2015;56:1048–1054.
31. Adams CWM, Abdulla YH, Torres EM, Poston RN. Periventricular lesions in multiple sclerosis: their perivenous origin and relationship to granular ependymitis. Neuropathol Appl Neurobiol 1987;13:141–152.
32. Machado-Santos J, Saji E, Tröscher AR, et al. The compartmentalized inflammatory response in the multiple sclerosis brain is composed of tissue-resident CD8+ T lymphocytes and B cells. Brain J Neurol 2018;141:2066–2082.
33. Zrzavy T, Hametner S, Wimmer I, Butovsky O, Weiner HL, Lassmann H. Loss of "homeostatic" microglia and patterns of their activation in active multiple sclerosis. Brain J Neurol 2017;140:1900–1913.
34. Lee NJ, Ha S-K, Sati P, et al. Spatiotemporal distribution of fibrinogen in marmoset and human inflammatory demyelination. Brain 2018;141:1637–1649.
35. Petersen MA, Ryu JK, Akassoglou K. Fibrinogen in neurological diseases: mechanisms, imaging and therapeutics. Nat Rev Neurosci 2018;19:283–301.
36. Alcázar A, Regidor I, Masjuan J, Salinas M, Alvarez-Cermeño JC. Axonal damage induced by cerebrospinal fluid from patients with relapsing-remitting multiple sclerosis. J Neuroimmunol 2000;104:58–67.
37. Vidaurre OG, Haines JD, Katz Sand I, et al. Cerebrospinal fluid ceramides from patients with multiple sclerosis impair neuronal bioenergetics. Brain J Neurol 2014;137:2271–2286.
38. Chiou B, Lucassen E, Sather M, Kallianpur A, Connor J. Semaphorin4A and H-ferritin utilize Tim-1 on human oligodendrocytes: a novel neuro-immune axis. Glia 2018;66:1317–1330.
39. Küry P, Nath A, Créange A, et al. Human endogenous retroviruses in neurological diseases. Trends Mol Med 2018;24:379–394.
40. Bevan RJ, Evans R, Griffiths L, et al. Meningeal inflammation and cortical demyelination in acute multiple sclerosis. Ann Neurol 2018;84:829–842.
41. Howell OW, Reeves CA, Nicholas R, et al. Meningeal inflammation is widespread and linked to cortical pathology in multiple sclerosis. Brain 2011;134:2755–2771.
42. Magliozzi R, Howell O, Vora A, et al. Meningeal B-cell follicles in secondary progressive multiple sclerosis associate with early onset of disease and severe cortical pathology. Brain 2007;130:1089–1104.
43. Engelhardt B, Carare RO, Bechmann I, Flügel A, Laman JD, Weller RO. Vascular, glial, and lymphatic immune gateways of the central nervous system. Acta Neuropathol (Berl) 2016;132:317–338.
44. Kooij G, Kopplin K, Blasig R, et al. Disturbed function of the blood-cerebrospinal fluid barrier aggravates neuro-inflammation. Acta Neuropathol (Berl) 2014;128:267–277.
45. Lassmann H, van Horssen J, Mahad D. Progressive multiple sclerosis: pathology and pathogenesis. Nat Rev Neurol 2012;8:647–656.
46. Lavisse S, Guillermier M, Hérard A-S, et al. Reactive astrocytes overexpress TSPO and are detected by TSPO positron emission tomography imaging. J Neurosci 2012;32:10809–10818.
47. Nutma E, Stephenson JA, Gorter RP, et al. A quantitative neuropathological assessment of translocator protein expression in multiple sclerosis. Brain 2019;142:3440–3455.
48. Wimberley C, Lavisse S, Brulon V, et al. Impact of endothelial 18-kDa translocator protein on the quantification of 18F-DPA-714. J Nucl Med 2018;59:307–314.
49. Chechneva OV, Deng W. Mitochondrial translocator protein (TSPO), astrocytes and neuroinflammation. Neural Regen Res 2016;11:1056–1057.
50. Moll NM, Rietsch AM, Thomas S, et al. Multiple sclerosis normal-appearing white matter: pathology-imaging correlations. Ann Neurol 2011;70:764–773.

Structural and Clinical Correlates of a Periventricular Gradient of Neuroinflammation in Multiple Sclerosis

Emilie Poirion, Matteo Tonietto, François-Xavier Lejeune, et al.

Neurology 2021;96;e1865-e1875 Published Online before print March 18, 2021
DOI 10.1212/WNL.0000000000011700